JMEPEG (2011) 20:1336–1345
DOI: 10.1007/s11665-010-9771-5

1059-9495/$19.00

Optimal Weld Parameters, Weld Microstructure, Mechanical Properties, and Hydrogen Absorption: An Effective Analysis

J. Bhattacharya and T.K. Pal

(Submitted February 10, 2010; in revised form July 23, 2010)

Weld bead-in-grooves were deposited on low alloy, high strength steel plates (ASTM A 517 Grade "F") with a commercial flux-cored filler wire, Auto-MIG 420, at different welding conditions. Microstructure and mechanical properties of welds were characterized by means of optical microscopy, SEM, TEM, EPMA, microhardness measurements, tensile tests, and Charpy impact tests. Hydrogen content of weld metals in as-weld condition and after exposing in simulated service condition was measured by LECO Gas Analyzer. Microstructure of weld metals consisted primarily of lath martensite with small amount of M-A constituents (Martensite-Austenite alternating layers). For some particular welding conditions, such as higher heat input and lower preheat temperatures etc., acicular ferrite is observed with lath martensite. Welds consisting of acicular ferrite in the microstructure showed improved mechanical properties as well as lower hydrogen absorption. The study provides guidelines for selecting proper welding conditions, which results in lower propensity to absorb hydrogen during service, as well as better mechanical properties. Necessity of post-weld heat treatment processes, which is mainly performed to achieve toughness, may be reduced; consequently saving cost and time of the welding process.

Keywords hydrogen absorption, low alloy high strength steel, mechanical property, microstructure, weld metal

1. Introduction

Fabrication industries always look for the development of light weight structures with cost-effective high productivity. Accordingly, low alloy steels with high strength are widely used in fabrication industries owing to their enough strength-to-weight ratios and comparatively lower cost. Thus, ASTM A 517 grade "F," a low alloy high strength steel, plays a greater role in manufacturing of earth moving equipments, penstocks, pressure vessels, bridges, scroll cases, steel mill equipments etc. Among different welding processes in fabrication of this steel (ASTM A 517 grade "F"), significance of flux-cored arc (FCA) welding is rapidly increasing because of its higher productivity. To minimize the frequent incidents of cold cracking in this high strength FCA weld metals, low hydrogen filler wire is used. Still, hydrogen embrittlement is a threatening problem in weld joints, particularly if it is exposed in hydrogenous atmosphere. The probability increases when weld metals become much harder than base metal by achieving higher amount of alloying elements from overmatching filler wires. However, in this process, as the strength of the weld metal improves, additional caution is to be taken during joining to achieve the required toughness criteria. Specifically, proper welding of this steel requires precise control of heat input and preheat/interpass temperatures to ensure the production of acceptable microstructures and requisite mechanical properties.

The microstructure of the low alloy steel weld metals generally consist of polygonal ferrite, grain boundary ferrite, widmanstatten ferrite, acicular ferrite, upper bainite, lower bainite, martensite, and M-A constituents (Ref 1, 2). As much as the carbon or alloying elements in the weld metal increases, there occurs consequential increase in lath martensite, bainite and acicular ferrite; replacing polygonal ferrite, grain boundary ferrite, and widmanstatten ferrite in the weld metal. This replacement results in enhanced strength. Low alloy steel weld metals with essentially lath martensite and bainite, can achieve the yield strength higher than 690 MPa but at the cost of toughness (Ref 3).

A common practice of recovering toughness and reducing the chances of cold cracking in weld metal is post-weld heat treatment. However, this process is not preferable for some of the low alloy high strength steel welds (Ref 4), specifically for ASTM A 517 grade "F." Moreover, post-weld heat treatment may produce some deterioration of impact properties in the transition temperature zone. This necessitates a different aspect of improving toughness in weld metal, other than post-weld heat treatment.

Control of microstructure may be considered as an alternative way of improving toughness in weld metal. Micro constituents such as acicular ferrite, with sufficient toughness, may increase toughness value in weld metal. During the past few decades, a number of efforts had been made to correlate the welding parameters, microstructure, and mechanical properties of weld metals (in different welding processes), though mostly on steels of low and moderate strength level (Ref 1, 5-8). Based on a research study on SMA weld metal of 850 MPa tensile

J. Bhattacharya and **T.K. Pal**, Metallurgical and Materials Engineering Department, Jadavpur University, Kolkata, India. Contact e-mail: jana_r_b@yahoo.co.in.

strength, Dixon and Hakansson (Ref 3) suggested combination of high preheat temperature and low welding heat input for achieving better toughness. On a different aspect, in SA welding process of HY 100 steel, researchers opined to keep preheat at minimum level and heat input at higher level, for attaining considerable savings in both time and money (Ref 3). However, suggested welding conditions for achieving suitable microstructure and other joint performances vary from process to process (Ref 9). Hence, an area of suitable welding conditions in FCA welding may worthfully be investigated to achieve necessary toughness when the joint is of high strength martensitic weld metals.

Besides toughness criteria, another crucial factor for high strength martensitic weld metal is to reduce property deterioration caused by hydrogen. The weld metals with nominal hydrogen intrusion during welding may develop a critical concentration of hydrogen by absorption process when exposed in hydrogenous atmosphere. In that case, the weld joints may face immature failure by hydrogen embrittlement (HE). Susceptibility to hydrogen embrittlement of high strength alloys is often estimated or compared through the level of hydrogen absorbed by the alloys for certain duration (Ref 10). For a certain loading condition, higher hydrogen absorption within a shorter period implies more probabilities to reach critical hydrogen concentration. Thus, the susceptibility to HE can be minimized by reducing the hydrogen absorption potential of weld metal. In this regard, it can be assumed that ferrite may absorb less amount of hydrogen than martensite as the apparent diffusivity of hydrogen in ferrite is higher than that of martensite (Ref 11). Therefore, under identical service conditions, more hydrogen is supposed to diffuse out from the ferrite than the martensite. Hence, susceptibility to hydrogen embrittlement may be reduced by small increase in ferrite percentage of martensitic weld metal, mechanical properties being kept at optimum level.

The present investigation was carried out to characterize the weld metal of ASTM A 517 grade "F" in such a way that the results can be utilized to find out a suitable area of welding conditions for obtaining a better toughness and precautionary microstructure for HE. At the same time, necessity of further post-weld heat treatment may be minimized.

2. Experimental Procedure

The base material used in this study was ASTM A 517 Grade "F" (quenched and tempered), low-alloyed steel (chemical composition is given in Table 1). Weld depositions were made in the grooves of $300 \times 150 \times 38$ mm steel plates. Commercial flux-cored filler wire (Auto-MIG 420) of 1.6-mm diameter and having slightly overmatching strength was chosen as consumable. The composition of the filler wire (given in Table 1) is close to filler wire grade E110T5-K4 (except Mn enrichment). Welding process opted was gas metal arc welding performed in automatic "Pro-MIG" equipment (Kempi make). Single bead-in-groove weld deposition was preferred to avoid the complexity in different zones of multipass weld joints. The groove design is shown in Fig. 1. 100% CO_2 at 15 L min^{-1} flow rate was used as shielding gas. Two different preheating temperatures—100 °C and 170 °C—were maintained during welding. Heat input was varied by using three current levels: 280, 350, and 400 A. A constant voltage of 26 V, a constant contact tip-work piece distance (CTWD) of 18 mm, and a horizontal travel speed of 30 cm min^{-1} were maintained throughout the welding. The detailed welding parameters are given in Table 2. With three current levels for two preheating temperatures each, six samples, viz. $M_1$1, $M_1$2, $M_1$3, $M_2$1, $M_2$2, and $M_2$3 were prepared (chemical compositions are given in Table 3).

After weld depositions were completed, all-weld tensile specimens, sub-size Charpy (transverse) specimens, and cross-sectioned metallographic specimens were prepared from the weld metals. Tensile test at 1 mm min^{-1} cross head speed and Charpy impact tests, at −51 °C as well as at room temperature, were done as per ASTM standard methods. Tensile strength of base metal and weld metals are given in Table 4. Charpy test data were converted to standard specimen values as per specification ASTM A 370-96 "Table 6" and illustrated in Table 5. SEM photographs at the fracture surface, 2 mm distant from the notch, inward of the Charpy specimens were recorded and given in Fig. 2(a)-(d).

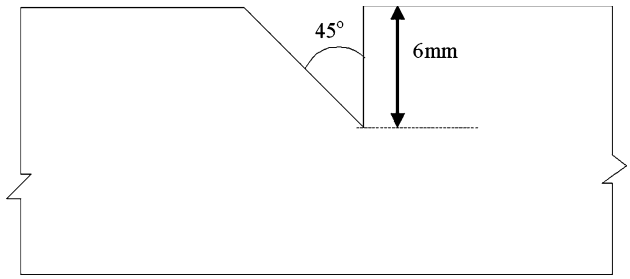

Fig. 1 Groove design for bead-in-groove deposit

Table 2 Different welding parameters

Sample No.	Preheat temp, °C	Current, A	Voltage, V	Heat input, kJ mm^{-1}
$M_1$1	100	280	26	1.24
$M_1$2	100	350	26	1.55
$M_1$3	100	400	26	1.77
$M_2$1	170	280	26	1.24
$M_2$2	170	350	26	1.55
$M_2$3	170	400	26	1.77

Table 1 Chemical composition of base metal and filler wire

	C, wt.%	Si, wt.%	Mn, wt.%	P, wt.%	S, wt.%	Cr, wt.%	Ni, wt.%	Mo, wt.%	Cu, wt.%	V, wt.%	B, wt.%
Base metal	0.18	0.27	0.76	0.035	0.035	0.4	0.7	0.4	0.3	0.05	0.003
Filler wire	0.035	0.348	2.51	<0.003	<0.003	0.309	2.6	0.647	0.12	0.019	<0.001
E110T5K4	0.15	0.8	1.2-2.25	0.03	0.03	0.2-0.6	1.75-2.6	0.3-0.65	…	0.05	…

Table 3 Chemical composition of the weld metals

Sample No.	C	Si	Mn	Cr	Ni	Mo	Cu	V	B
$M_1$1	0.077	0.265	1.64	0.338	2.22	0.492	0.144	0.024	<0.001
$M_1$2	0.056	0.227	1.37	0.305	2.35	0.443	0.127	0.018	<0.001
$M_1$3	0.069	0.25	1.59	0.324	2.25	0.480	0.136	0.02	<0.001
$M_2$1	0.087	0.239	1.46	0.313	2.26	0.467	0.17	0.023	<0.001
$M_2$2	0.073	0.232	1.56	0.324	2.2	0.492	0.157	0.019	<0.001
$M_2$3	0.072	0.238	1.55	0.317	2.24	0.481	0.162	0.021	<0.001

Table 4 Tensile strength and hardness of weld metals

Sample No.	0.2% PS, MPa	UTS, MPa	Hardness, VPN
Base metal	695	854	261
$M_1$1	785	1182	388
$M_1$2	778	1161	380
$M_1$3	778	1171	385
$M_2$1	715	996	331
$M_2$2	732	1066	351
$M_2$3	770	1141	370

Table 5 Charpy impact values of different weld metals and base metal

Sample No.	Impact toughness (J) at room temperature	Impact toughness (J) at −51 °C
$M_1$1	60	54
$M_1$2	68	62
$M_1$3	52	48
$M_2$1	80	76
$M_2$2	72	64
$M_2$3	40	40
Base	162	136

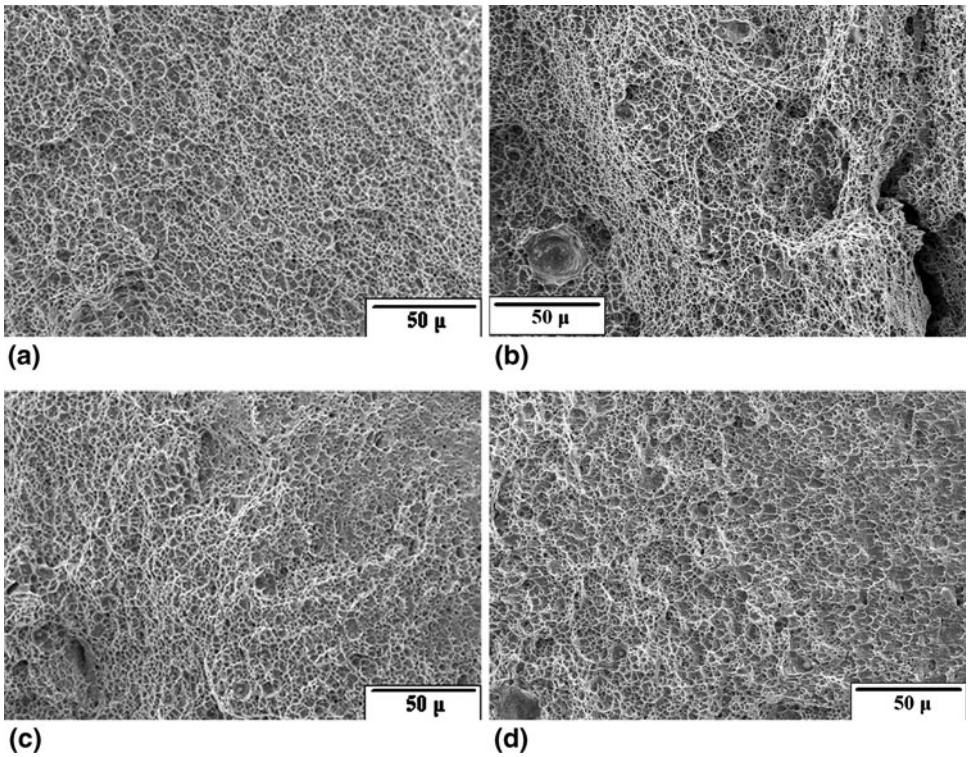

Fig. 2 SEM photograph at fracture surface, 2 mm distant from the notch of Charpy specimens (a) $M_1$3 tested at room temperature, (b) $M_1$3 tested at −51 °C, (c) $M_2$1 tested at room temperature, and (d) $M_2$1 tested at −51 °C

The metallographic specimens of all the weld metals were initially etched with 2% nital to study the weld profiles (Fig. 3a, b) as well as the microstructure of base metal, HAZ, and weld metals (Fig. 4, 5). Then, average diameters of base metal grains and weld metal columnar grains were measured. Thereafter, the specimens were re-polished and etched with Le Pera's reagent (which is a fresh solution of 4% picric acid in ethanol mixed with a 1% solution of sodium metabisulfite in distilled water in 1:2 volume ratio) (Ref 12) for further detailed study of microstructure (Fig. 6-8). This etchant generally tints the bainite as dark brown, ferrite as tan, tempered martensite as black, and leaves retained austenite and untempered martensite alone and unaffected (Ref 12). Microstructures of all the weld metals were quantified using Axio Image Analyzer (Carl Zeiss)

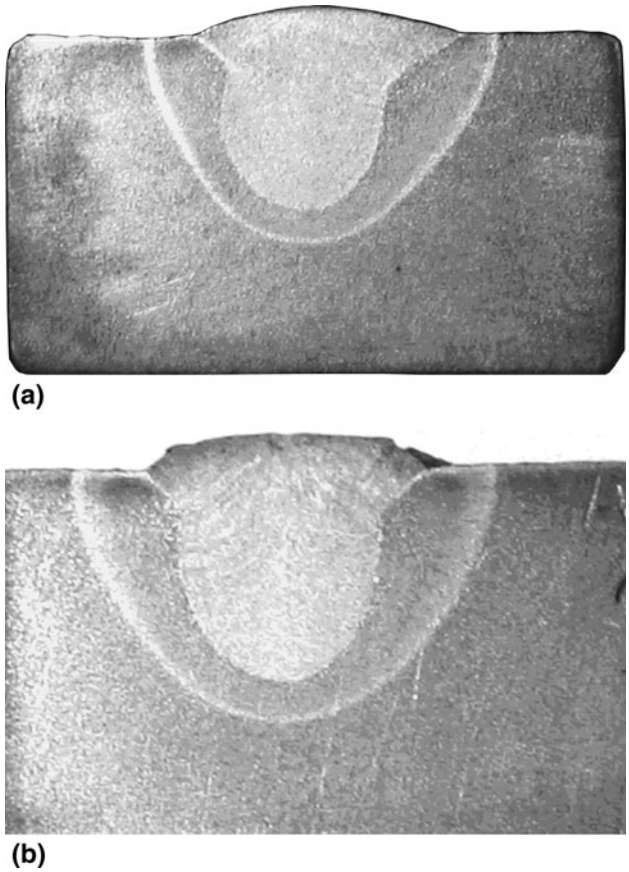

Fig. 3 Photomacrograph of weldments showing weld profile (a) $M_1 2$ and (b) $M_2 2$

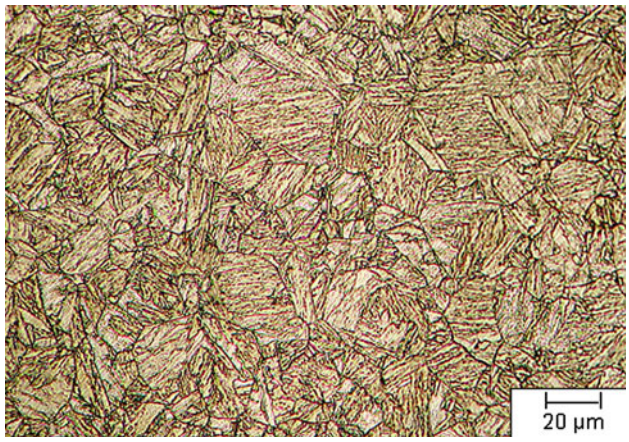

Fig. 4 Microstructure of base metal

and are illustrated in Table 6. In addition to optical metallography, Field Emission Gun Scanning Electron Microscope (SEM), Energy Dispersive Spectroscopy (EDS), Transmission Electron Microscopy (TEM), Electron Probe Micro Analysis (EPMA), and microhardness measurements were performed to characterize the weld metals. Average hardness was taken by Vicker's hardness tester.

To measure the hydrogen content in as-welded metal, $50 \times 50 \times 38$ mm blocks with similar "V" groove were filled with weld deposit, and immediately after weld deposition, they

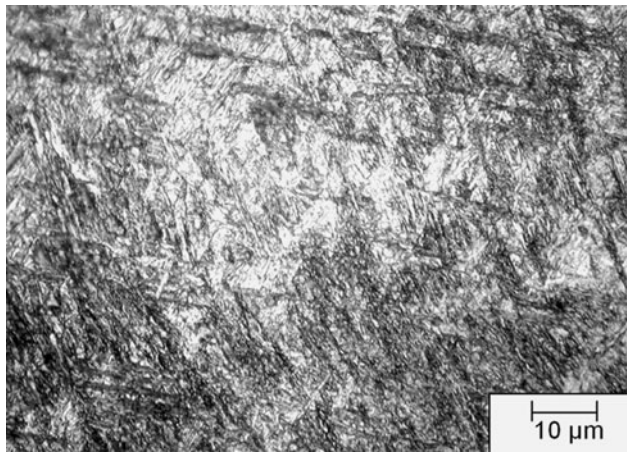

Fig. 5 Microstructure of weld metal $M_1 3$ (2% Nital), revealing lath martensites within the columnar grains

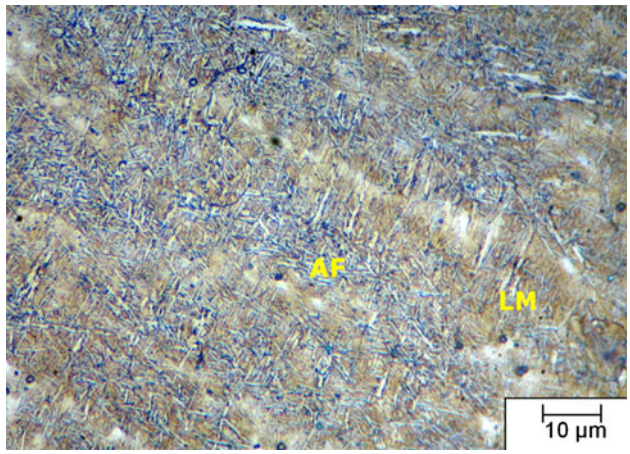

Fig. 6 Microstructure of weld metal $M_1 2$ revealing essentially lath martensite with some acicular ferrite

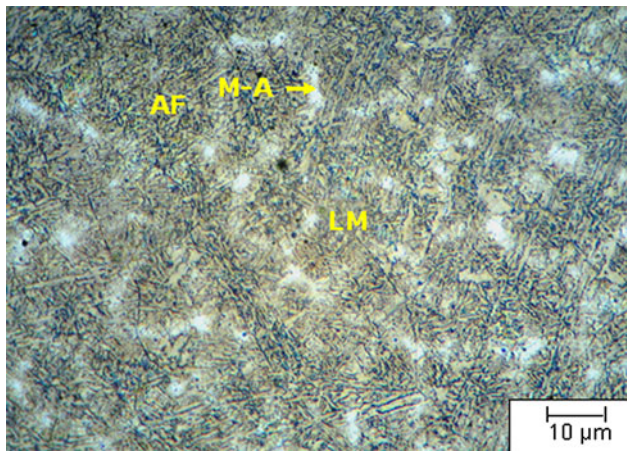

Fig. 7 Microstructure of weld metal $M_2 1$ revealing lath martensite, acicular ferrite and M-A constituents

were immersed in liquid nitrogen to immobilize the absorbed hydrogen. Small cylindrical specimens (∅ 10 mm × 3 mm) were prepared from the blocks in special cooling atmosphere and were tested in LECO Gas Analyzer. Thus, hydrogen

content in as-weld condition was measured and listed in Table 7. Further, critical service condition of weld joints was simulated in laboratory by continuous cathodic charging of hydrogen on weld metal surface under slow strain rate tensile loading. Single edge-notched (SEN) specimens were prepared to obtain notch effect in the simulated condition. The specimens were stressed under continuous tensile load and hydrogen was charged cathodically at the notched portions for 80 h followed by immediate immersion of the specimen in liquid nitrogen. From the notch area, which has experienced the maximum triaxial stresses, ∅ 10 mm × 3 mm cylindrical specimens were prepared for hydrogen measurement. The total absorbed hydrogen under above condition was measured by LECO Gas Analyzer as given in Table 7.

3. Results

Tensile strength and Vicker's hardness data of the base metal and weld metals—$M_1$1, $M_1$2, $M_1$3, $M_2$1, $M_2$2, and $M_2$3 are illustrated in Table 4. Tensile strength of the weld metals is considerably higher than the base metal. Sample No. $M_2$1 possesses the lowest UTS, 996 MPa, and Sample No. $M_1$1 possesses the highest UTS, 1182 MPa. Accordingly, Vicker's hardness values maintain the same trend of the tensile strength. Toughness value of the weld metals varies from 40 to 80 J at room temperature and 40-76 J at subzero temperature (Table 5). Among the weld metals, Sample No. $M_2$1 possesses the maximum toughness, and Sample No. $M_2$3 shows the minimum at both the test temperatures.

Microstructure of the base metal comprises mainly tempered martensite and bainite, and microstructure of the weld metals consists of predominantly lath martensite with different percentages of acicular ferrite and M-A constituents as illustrated in Table 6. A dendritic type of substructure is noticed throughout the weld metal microstructure (Fig. 4). In sample nos. $M_1$2, $M_2$1, and $M_2$2, percentage of acicular ferrite, observed within the dendrites (Fig. 6-8) are 10.4, 29.3, and 13.8%, respectively, whereas Sample Nos. $M_1$1, $M_1$3, and $M_2$3 contain negligible amount of acicular ferrite (Fig. 5). M-A constituents are observed at the core of the interdendritic regions in a scattered manner (Fig. 6, 7). Maximum percentage of M-A constituents (7.64%) is observed in Sample No. $M_2$1. However, there is little variation in the amount of M-A constituents of other weld metals (2.1-3.5%). The average columnar grain diameter varied from 47.65 to 73.51 μm in different weld metals (Table 6). The average interdendritic spacing, measured at the intermediate position from fusion boundary to centre line of the weld metal

Table 7 Hydrogen content in as-weld metals and hydrogen charged stressed weld metals

Sample No.	Hydrogen content, ppm	
	As welded	After charging 80 h and loading up to 550 kg
$M_2$1	2.35	10.5
$M_2$2	2.51	11.2
$M_2$3	2.41	11.8

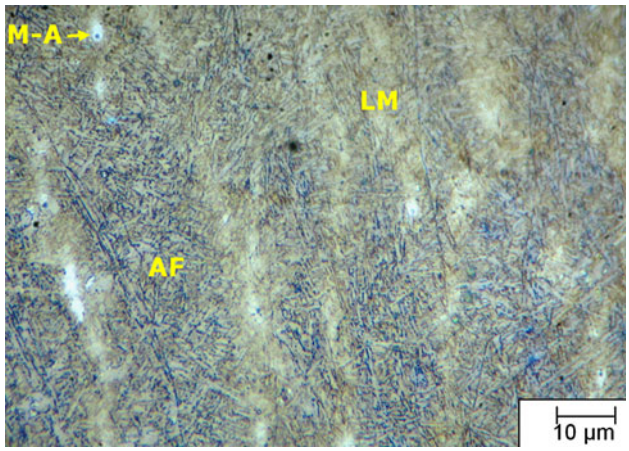

Fig. 8 Microstructure of weld metal $M_2$2 revealing lath martensite, acicular ferrite and M-A constituents

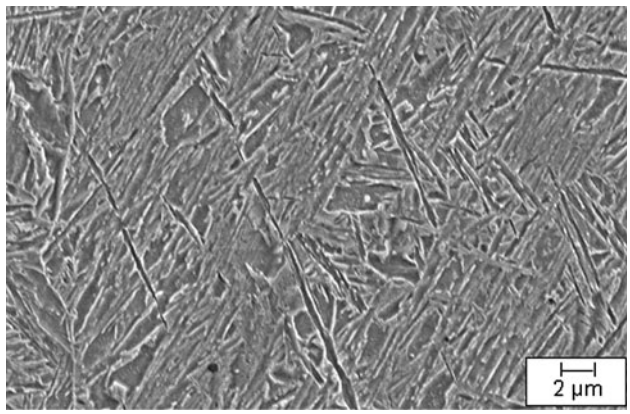

Fig. 9 FEGSEM photograph of lath martensite

Table 6 Microstructural details of the base metal and weld metals

Sample	Columnar grain dia., μm	Interdendritic spacing, μm	Microstructure	% M-A const.	% AF	% vol. frac. of inclusion	Avg. width of LM	Avg. width of AF
Base	40		Tempered B + M				0.6-0.8	
$M_1$1	47.65	17.7	LM + M-A const.	2.1	Neg.	0.611	0.6-0.8	…
$M_1$2	52.9	20.62	LM + AF + M-A const.	3.5	10.4	…	0.8-1	0.75
$M_1$3	70	29.16	LM + M-A const.	2.2	Neg.	…	1-1.4	…
$M_2$1	52.09	19.86	LM + AF + M-A const.	7.64	29.3	0.623	1-1.4	1.24
$M_2$2	64	25.3	LM + AF + M-A const.	3.1	13.8	…	1.2-1.6	1.25
$M_2$3	73.51	39.98	LM + M-A const.	2.5	Neg.	0.642		…

was observed to vary from 17.7 to 39.98 μm (Table 6). The lath shape of martensite in weld metal is well defined in Fig. 9, as revealed by FEGSEM study.

Average diameter of the inclusions varied from 1.2 to 2.3 μm as obtained by TEM photographs (Fig. 10). Volume fractions of the inclusions were observed to be similar in all the weld metals as presented in Table 6. The composition of inclusions in weld metals as detected by TEM with EDS facility was Fe-Al-Mn-Ti oxide type (Fig. 11). The width of martensite laths varied from 0.6 to 1.6 μm and the width of acicular ferrite varied from 0.75 to 1.25 μm (Table 6) as studied by SEM and TEM.

Fig. 10 TEM Photograph of weld metal M_21 revealing lath martensite and the acicular ferrite nucleated from inclusions

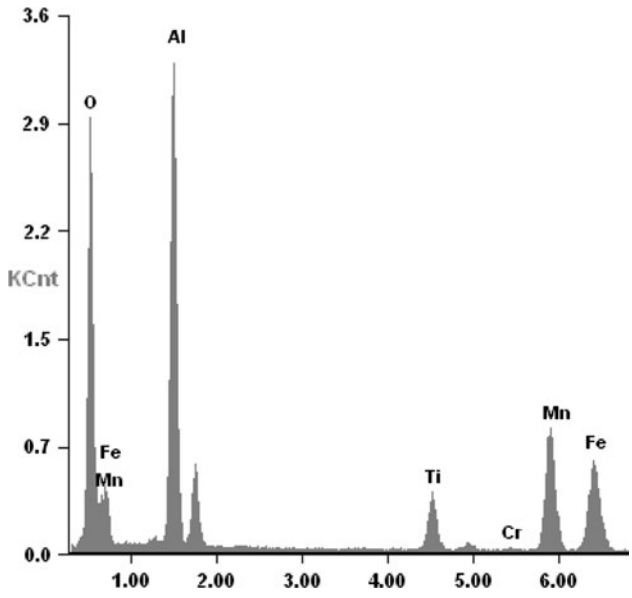

Fig. 11 EDS analysis of an inclusion shown in Fig. 10

Microhardness in the weld metals varied from 311 to 394 HV (Fig. 12a, b). The average hardness of acicular ferrite, martensite, and M-A constituents, measured using 10 gm load, were 280, 380, and 425 HV, respectively.

In order to study the degree of micro-segregation in weld metals, electron probe micro analysis (EPMA) test at the intermediate region of fusion boundary and the weld center line (marked in Fig. 13a) were carried out. EPMA test data in terms of weight percentages of alloying elements were plotted against the distance traversed at 4-μm intervals which are shown in Fig. 13(b). Segregation of Mn, Ni, and Mo is observed to be predominant at some spots within a certain interval in the weld metals. Further, percentages of all these alloying elements at micro-segregation are 1.1-1.6 times higher than average compositions in weld metals.

A little variation in the hydrogen content of as-welded metals was observed and the amounts of hydrogen were within the specified level of low hydrogen electrodes (2-5 mL/100 g or 1.78-4.46 ppm) (Ref 13). After 80 h of hydrogen charging under tensile load, the hydrogen content in weld metals was observed to increase in the range of 10.5-11.8 ppm (Table 7).

4. Discussion

The commercial electrode compositions are typically designed in such a way that little variations in welding condition could not be able to make any significant change in weld properties. In this study, a wide range of deviation in the property of weld metal as well as variations in microstructure is observed with small deviation of welding conditions. It indicates that the weld metal possessing this typical composition is quite sensitive to the changes in thermal cycles.

To understand the different microstructural transformation behavior occurred in the weld metals, thermal cycles were evaluated from modified Rosenthal equations (Ref 14) as follows:

$$T - T_0 = \frac{q_0}{2\pi\lambda}\left(\frac{1}{R}\right)\exp\left[-\frac{\nu}{2a}\right](R + x)$$

$$\Delta\tau = n_3\left(\frac{1}{\theta_2} - \frac{1}{\theta_1}\right)$$

where T_0 = Preheat temperature, q_0 = Net power received by weldment (W), λ = Thermal conductivity (W mm^{-1} °C^{-1}), ν = Weld speed (mm s^{-1}), a = Thermal diffusivity (mm^2 s^{-1}), R = Radial distance of the point of interest from power source, X = v.t, $\Delta\tau$ = Cooling time within two specific temperatures θ_2 and θ_1, and n_3 = dimensionless operating parameter.

Cooling times ($\Delta\tau$) at different temperature intervals for all the six samples were evaluated from these equations (Ref 14) and is given in Table 8. A schematic diagram of the weld metal cooling curves from solidification temperature, derived by the said equations, is shown in Fig. 14.

Differences in interdendritic spacing and grain diameter suggest that microstructural variations start from solidification process. Thermal cycle above grain boundary dissolution temperature is responsible for grain coarsening in HAZ, and this HAZ grain in turn decides the primary grain diameter of the weld metal at fusion boundary. Hence, cooling time just below solidification temperature (1520 °C) (Ref 14) and the

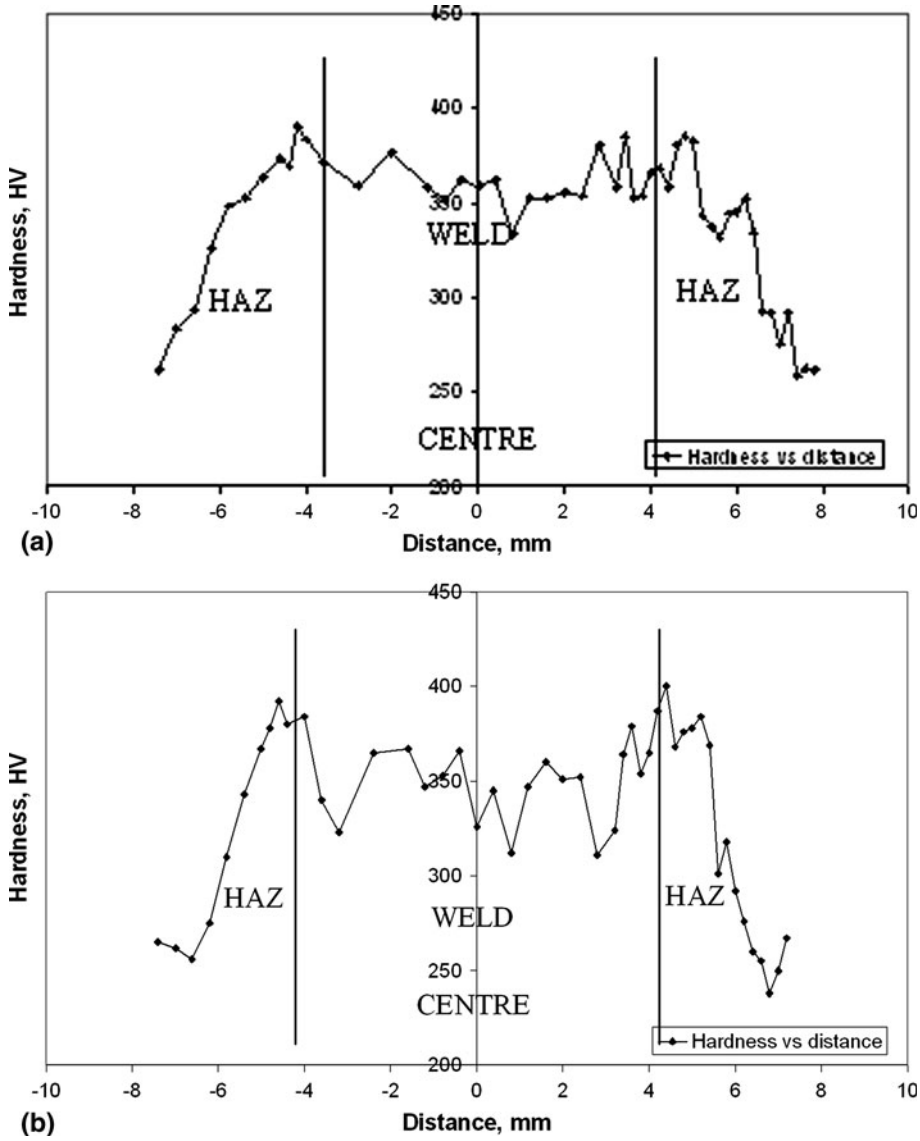

Fig. 12 Microhardness of weldments (a) $M_1$1 and (b) $M_2$1

solidification time are effectively responsible for the characteristics of grain structure in weld metal. It may be observed from Table 8 and Fig. 14 that the weld metals ($M_1$1, $M_1$2, $M_1$3, $M_2$1, $M_2$2, and $M_2$3) are ordered as $M_1$1, $M_2$1, $M_1$2, $M_2$2, $M_1$3, and $M_2$3 according to their increasing cooling time or decreasing cooling rate at solidification temperature as well as within the temperature region from 1520 to 1300 °C. Consequently, the prior austenite grain diameter of these weld metals increases from 47.65 to 73.51 μm directly with the decreasing order of cooling rate at this temperature region. Again, dendritic structure of weld metals takes shape at the time of solidification. In this study, interdendritic spacing varies from 17.7 to 39.98 μm (Table 6) directly proportional with the order of cooling rate (Table 8) at solidification temperature (1520 °C). Here, in this study, the increasing order of austenitic grain diameter and interdendritic spacing of the weld metals indicate that the effect of welding current is more predominant on cooling rate at higher temperature region (≥1300 °C).

On further cooling, at different temperatures within the range 800-300 °C, austenite starts to decompose into different micro-constituents; such as acicular ferrite, bainite and martensite, depending on the factors—cooling rate, prior austenite grain size and composition. Base metal composition (Table 1) was developed in such a way that on quenching, its microstructure consists of bainite and martensite. However, by the dilution of base metal with filler wire, weld metals lose its carbon content and achieve enrichment of alloying elements (Table 3). Increase in Mn and Ni changes the microstructure from bainite plus martensite in base metal to essentially lath martensite in weld metals. Suppression of bainite is considered to be due to typical weld metal composition, where there is a narrow difference between B_s temperature and M_s temperature (Table 9). The approximate value of B_s temperature and M_s temperature of weld metal is calculated from the equations summarized by Akselsen and Simonsen (Ref 15). The amount of martensite generally increases with the order of the cooling rate prevailing at M_s temperature. Here, order of the weld metals as per decreasing cooling rate within the range 500-300 °C is $M_1$1, $M_1$2, $M_1$3, $M_2$1, $M_2$2, and $M_2$3. However, surprisingly in this study, the percentage of martensite in the

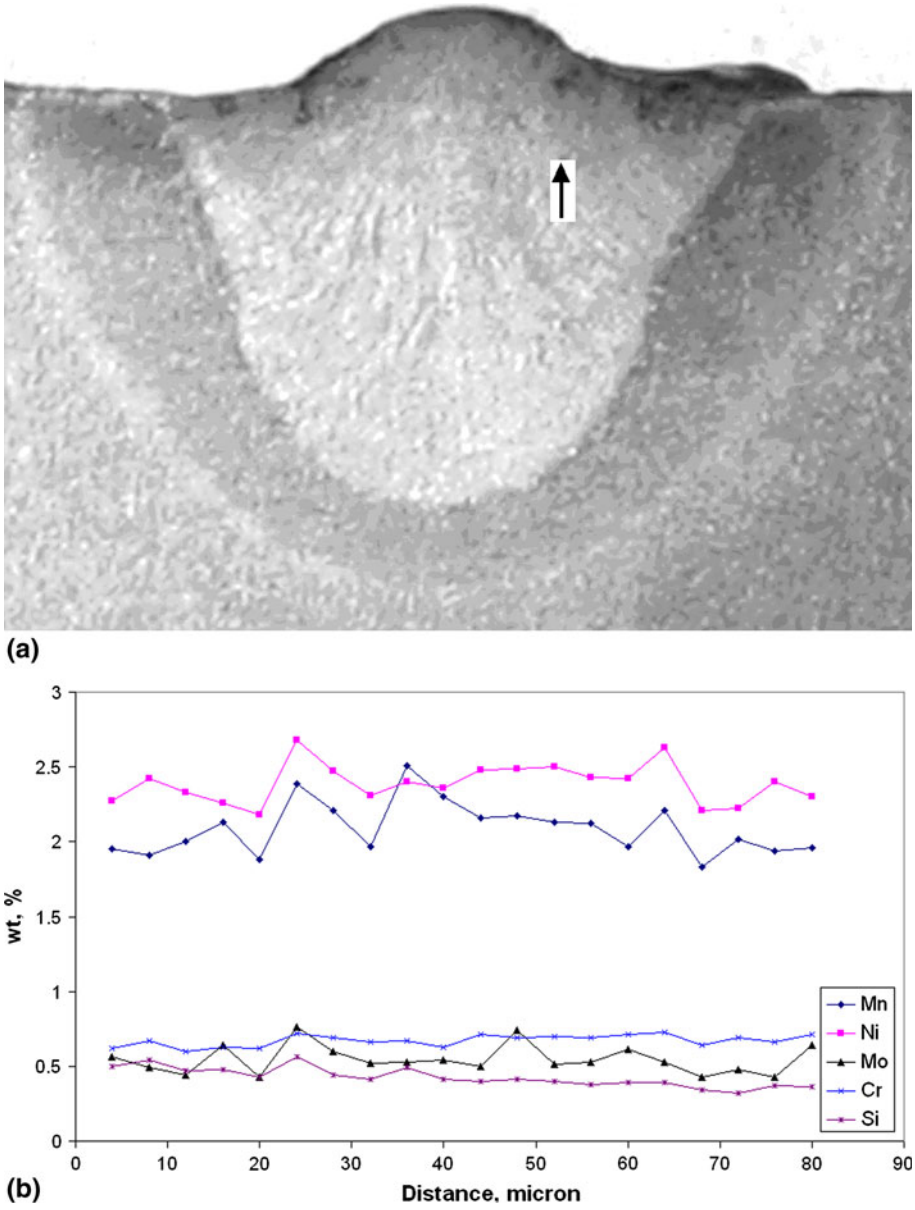

Fig. 13 (a) Location and direction of EPMA at weld metals $M_1$1, (b) percentage of elements vs. distance plot showing alloy enrichment at certain intervals

Table 8 Cooling time of different temperature zones

Sample No.	$\Delta\tau_{solidification}$, s	$\Delta\tau_{1520\text{-}1300}$, s	$\Delta\tau_{800\text{-}500}$, s	$\Delta\tau_{500\text{-}300}$, s
$M_1$1	1.56	2.54	21.11	49.27
$M_1$2	1.95	3.17	26.39	61.59
$M_1$3	2.34	3.63	30.16	70.39
$M_2$1	1.73	2.85	28.42	91.89
$M_2$2	2.16	3.56	35.53	114.86
$M_2$3	2.59	4.07	40.61	131.27

weld metals does not follow the order. The results, however, show some deviations from usual correlation and interestingly these deviations can be justified when both cooling rate and grain size are taken into consideration. For example; Sample No. $M_2$3, having largest austenitic grain diameter (73.51 μm)

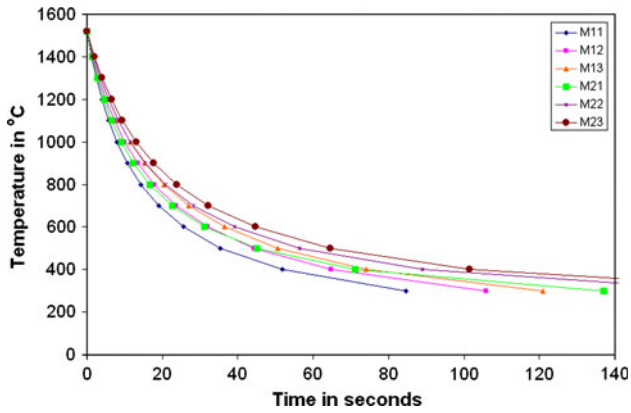

Fig. 14 Schematically presented thermal cycles of the weld metals (from solidification temperature)

Table 9 Approximate values of M_s and B_s temperature

Average calculated temperature	Weld metal		
	Non-segregated areas	Segregated areas	Base
M_s, °C	419	365	423
B_s, °C	546	383	626

and slowest cooling rate ($\Delta\tau_{800\text{-}500}$ = 40.61 s), possesses mainly lath martensite with negligible amount of acicular ferrite, whereas Sample No. $M_2$1, having grain diameter 52.09 μm and experiencing slightly faster cooling rate ($\Delta\tau_{800\text{-}500}$ = 28.42 s) possesses highest percentage of acicular ferrite (29.3%). It is observed from Table 6 and 8 that weld metal with relatively smaller austenitic grains possesses relatively higher amount of acicular ferrite even if it experienced relatively faster cooling rate. This feature of the weld metal is quite justified as smaller austenitic grains promote earlier transformation of austenite and thus provide longer duration for transformation of austenite into acicular ferrite above M_s temperature (419 °C). Accordingly, larger austenitic grain size lowers the transformation temperature close to M_s temperature and suppresses ferritic transformation (Ref 16). Hence, percentages of acicular ferrite and martensite in weld metals are determined collectively by prior austenite grain size and cooling rate (Table 6, 8). Although, a direct effect of higher cooling rate at solid transformation temperature is observed as reduction in acicular ferrite width and the lath martensite width at their respective transformation temperature. According to the increasing coarseness of lath martensite and acicular ferrite, the weld metals can be ordered as $M_1$1, $M_1$2, $M_1$3, $M_2$1, $M_2$2, $M_2$3 (Table 6) which matches with the order of decreasing cooling rate in the temperature range 500-300 °C (Table 8). The order of arrangement of weld metals, i.e., $M_1$1, $M_1$2, $M_1$3, $M_2$1, $M_2$2, $M_2$3 also indicates that in comparison with heat input, preheat temperature has more prominent effect on the cooling rate in the temperature range 500-300 °C. Furthermore, similar volume fraction of oxide inclusion in the weld metals indicates that there is little effect of inclusion on variation in percentage of acicular ferrite. However, Sample No. $M_1$1, which shows a different behavior, may be the case where too fast cooling rate suppresses the grain size effect and becomes responsible for formation of fine lath martensite (0.6-0.8 μm width) without any considerable amount of acicular ferrite.

Core of the microsegregated dendritic arms, which attained the highest alloy enrichment because of alloy partition during solidification process, finally transforms to M-A constituents. It is the combination of lenticular or micro-twined martensite with some retained austenite and precipitated carbides, formed in alternating layers (Ref 17). This composition with highest alloy enrichment results in high microhardness value of 425 HV. Higher percentage of M-A constituents (7.64%) in Sample No. $M_2$1 is a result of transformation of carbon-enriched austenite, retained in acicular ferrite region.

Tensile strength as well as hardness of the weld metals has an inverse relationship with the amount of acicular ferrite in lath martensitic microstructure. Further, coarseness of the structure exerts considerable effect on tensile properties and hardness. Expectedly, Sample No. $M_2$1, having lath martensite with the highest amount of acicular ferrite (29.3%) possesses the lower tensile strength and hardness (996 MPa and 331 HV) compared to Sample No. $M_2$2 which has a smaller amount of

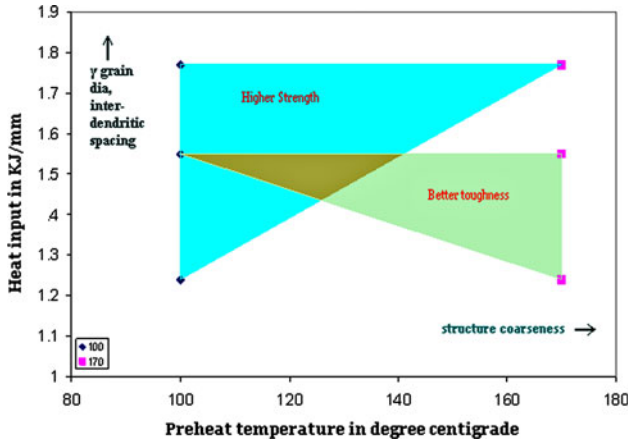

Fig. 15 Schematically presented effect of preheat temperature and heat input on weld properties

acicular ferrite, and thereby possesses higher strength and hardness (1066 MPa and 351 HV). On the other hand, sample nos. $M_1$1, $M_1$3, and $M_2$3 (arranged in the order of increasing coarseness), having similar microstructure with negligible amount of acicular ferrite show gradual decrease in the tensile strength (1182, 1171, and 1141 MPa, respectively) and hardness (388, 385, and 370 HV) as an effect of coarseness of the lath martensite (Table 4).

The toughness increases mainly with increasing amount of acicular ferrite in weld metals. Toughness is also affected by the amount of M-A constituents present in the weld metals. As expected, Sample No. $M_2$1, having the highest amount of acicular ferrite (29.3%) shows the maximum impact toughness both at room temperature and subzero temperature (Table 5). The variation in values of toughness among the present samples is attributed to combined effect of variation in coarseness of the structure as well as percentage of M-A constituents. Specifically, toughness decreases as coarseness increases in weld metals and, since M-A constituents are brittle in nature, it has the same effect on toughness of weld metals. SEM fractograph at same distance from notch of the Charpy specimen shows onset of cleavage fracture region which is most prominent in Fig. 2(b).

In comparison of mechanical properties between base metal and weld metals (Table 4, 5), higher tensile strength and lower toughness of weld metal are attributed to its higher hardenability caused by increased percentage of Mn and Ni content.

Based on the present investigation, welding conditions providing higher strength and better toughness are marked schematically in Fig. 15. The common region in between triangular area of higher strength and triangular area of better toughness shows superior combinations of strength and toughness. It opens the scope of further research study to distinctly mark the boundary conditions for optimum strength-toughness combination, by carrying out a series of experiments. Correlation between austenitic grain size and heat input, as well as structure (martensite, acicular ferrite) coarseness and preheat temperature, is also presented in this figure.

Hydrogen content of the weld metals at as-welded condition varies in a narrow range, 2.35-2.51 ppm, whereas, after allowing 80 h to absorb hydrogen in the weld metals at similar loading condition, hydrogen content differs in comparatively wider range, 10.5-11.8 ppm. It indicates a major role of in-built microstructure in the absorption of hydrogen into the weld metals. As the apparent diffusivity of hydrogen in steel is

higher in ferritic component than a martensitic component (Ref 11), it can be expected that, under an identical service condition, less hydrogen should diffuse out from a martensitic weld metal than a ferritic weld metal. In the present investigation, Sample No. $M_2$1 with the highest percentage of acicular ferrite shows lowest amount of hydrogen absorption (Table 7), indicating the minimum susceptibility to hydrogen embrittlement. With the same logic, maximum susceptibility to HE may be expected in Sample No. $M_2$3 which has the maximum tendency to absorb hydrogen because of presence of negligible amount of acicular ferrite.

Comparing the mechanical properties and hydrogen absorption, it is observed that combination of higher preheat temperature (170 °C) and lower heat input (280 A current) provides the maximum toughness and minimum hydrogen absorption, but the lowest tensile strength—as in Sample No. $M_2$1. A good combination of higher strength, moderate toughness and lower hydrogen absorption is obtained from higher preheat temperature (170 °C) with intermediate heat input (350 A current)—as in Sample No. $M_2$2 and at lower preheat temperature (100 °C) with intermediate heat input (350 A current)—as in Sample No. $M_1$2.

5. Conclusion

Combination of higher preheat temperature (170 °C)-lower heat input (280 A current), higher preheat temperature (170 °C)-intermediate heat input (350 A current), and lower preheat temperature (100 °C)-intermediate heat input (350 A current) provides better weld performance. Combination of low preheat temperature (100 °C) with low heat input (280 A current) or high preheat temperature (170 °C) with high heat input (400 A current) results in poor quality of weld metals.

It may also be concluded that austenitic grain diameter and interdendritic spacing are predominantly controlled by heat input, whereas, microstructure coarseness is dependent mostly on preheat temperature rather than heat input.

Minimum hydrogen absorption as well as improved toughness may be obtained by allowing acicular ferrite formation in martensitic weld metal but at the cost of tensile strength. According to service requirements, optimum combination of strength, toughness, and HE resistance may be attained by proper selection of welding parameters. This may effectively reduce the applicability of post-weld heat treatment, and hence increase productivity.

Acknowledgments

The authors are thankful to the Council of Scientific and Industrial Research (CSIR) for sponsoring this research study. The authors also express thanks to Dr. P. C. Chakrabarty, Head of the Department, Metallurgical & Material Engineering Department, Jadavpur University, for his prompt support of instrumental facilities.

References

1. O. Grong and D.K. Matlock, Microstructural Development in Mild Steel and Low-Alloy Steel Weld Metals, *Int. Met. Rev.*, 1986, **31**(1), p 27–48
2. J.C.F. Jorge, L.F.G. Souza, and J.M.A. Rebello, The Effect of Chromium on the Microstructure/Toughness Relationship of C-Mn Weld Metal Deposits, *Mater. Charact.*, 2001, **47**, p 195–205
3. B. Dixon and K. Hakansson, Effect of Welding Parameters on Weld Zone Toughness and Hardness in 690 MPa Steel, *Weld. Res. Suppl.*, 1995, **74**, p 122s–131s
4. American Welding Society, Low Alloy Steel, *AWS Welding Handbook—Metals and Their Weldability*, Sec. 4, 6th ed., American Welding Society, Miami, 1972, p 63.11–63.36
5. S.D. Bhole, J.B. Nimade, L. Collins, and C. Liu, Effect of Nickel and Molybdenum Additions on Weld Metal Toughness in a Submerged arc Welded HSLA Line Pipe Steel, *J. Mater. Process. Technol.*, 2006, **173**, p 92–100
6. Z. Zhang and R.A. Farrar, Influence of Mn and Ni on the Microstructure and Toughness of C-Mn-Ni Weld Metals, *Weld. Res. Suppl.*, 1997, **76**, p 183-s–196-s
7. J.C. Gonzalez, L.A. de Vedia, and H. Biloni, *Development of a High Strength Gas Shielded FCAW Electrode for High Toughness Applications*, Vol XII-986-86, Instituto Argentino De Siderurgia, International Institute of Welding, 1986
8. B. Basu and R. Raman, Microstructural Variations in a High-Strength Structural Steel Weld Under Isoheat Input Conditions, *Weld. J.* 2002, **81**, p 239s–248s
9. G. Atkins, D. Thiessen, N. Nissley, and Y. Adonyi, Welding Process Effects in Weldability Testing of Steels, *Weld. J.*, 2002, **81**, p 61-s–68-s
10. B.G. Pound, *Evaluation of a Diffusion/Trapping Model for Hydrogen Ingress in High Strength Alloys*, Annual Report, SRI International, November, 1994
11. S.K. Albert, V. Ramasubbu, N. Parvathavarthini, and T.P.S. Gill, Influence of Alloying on Hydrogen-Assisted Cracking and Diffusible Hydrogen Content in Cr-Mo Steel Welds, *Sadhana*, 2003, **28**, p 383–393
12. Y.D. Park, I.S. Maroef, A. Landau, and D.L. Olson, Retained Austenite as a Hydrogen Trap in Steel Welds, *Weld. J.*, 2002, **81**, p 27s–35s
13. J.F. Lancaster, *Carbon and Ferritic Alloy Steels, Metallurgy of Welding*, 5th ed., Chapman & Hall, London, 1993, p 211
14. O. Grong, *Heat Flow and Temperature Distribution in Welding, Metallurgical Modelling of Welding*, The Institute of Materials, London, 1994, p 1–40
15. O.M. Akselsen and T. Simonsen, Techniques for Examining Transformation Behaviour in Weld Metal and HAZ, *Indian Weld. J.*, 1988, **21**, p 344–349
16. M. Shome and O.N. Mohanty, Continuous Cooling Transformation Diagrams Applicable to the Heat Affected Zone of HSLA-80 and HSLA-100 Steels, *Metall. Mater. Trans. A*, 2006, **37A**, p 2159–2169
17. S. Shanmugam, N.K. Ramisetti, R.D.K. Misra, J. Hartmann, and S.G. Jansto, Microstructure and High Strength-Toughness Combination of a New 700 MPa Nb-Microalloyed Pipeline Steel, *Mater. Sci. Eng. A*, 2008, **478**, p 26–37